Article

Assessment of Bone Mineral Density from Lumbosacral MRI: A Retrospective Study with Texture Analysis Radiomics

Giulio Vara [1],* , **Paolo Spinnato [2]** , **Giancarlo Facchini [2]** , **Marco Miceli [2]** , **Francesco Ursini [3]** , **Luca Spinardi [4]** , **Gianfranco Vornetti [5]** and **Stefano Ratti [6]**

[1] Diagnostic and Interventional Radiology, Ospedale Civile "Umberto I", 70033 Lugo, Italy
[2] Diagnostic and Interventional Radiology, IRCCS Istituto Ortopedico Rizzoli, 40136 Bologna, Italy; paolo.spinnato@ior.it (P.S.); giancarlo.facchini@ior.it (G.F.); marco.miceli@ior.it (M.M.)
[3] Department of Biomedical and NeuroMotor Sciences (DIBINEM), University of Bologna, 40126 Bologna, Italy; francesco.ursini@ior.it
[4] IRCCS Azienda Ospedaliero-Universitaria di Bologna, 40138 Bologna, Italy; luca.spinardi@aosp.bo.it
[5] IRCCS Istituto delle Scienze Neurologiche di Bologna, 40139 Bologna, Italy; gianfranco.vornetti@unibo.it
[6] Cellular Signalling Laboratory, Department of Biomedical and NeuroMotor Sciences (DIBINEM), University of Bologna, 40126 Bologna, Italy; stefano.ratti@unibo.it
* Correspondence: giulio.vara@gmail.com; Tel.: +39-320-262-7412

Abstract: Osteoporosis is a common condition characterized by low bone mineral density (BMD) and deterioration of bone microarchitecture, leading to increased risk of fractures. Early diagnosis and treatment of osteoporosis are critical for preventing fractures and their associated morbidity and mortality. Currently, dual-energy X-ray absorptiometry (DXA) is the gold standard for assessing BMD; however, it has limitations such as radiation exposure, cost, and limited availability in certain regions. Magnetic resonance imaging (MRI) of the lumbar spine is routinely performed for various indications, and it provides high-resolution images of the bone and tissue without ionizing radiation. Recently, texture analysis (TA) of MRI images has shown promise in assessing BMD by quantifying the spatial distribution and heterogeneity of bone marrow fat and trabecular bone. In this article, we present our experience with the opportunistic use of lumbar spine MRI for BMD assessment using TA, and we compare the results with DXA measurements. We also discuss the potential clinical implications of this approach, including its use in patients who cannot undergo DXA or in whom BMD assessment is not routinely performed. MRI should provide information in a single examination in regard to degenerative disk pathology and arthritis, with the addition of BMD prediction.

Keywords: texture analysis; radiomics; osteoporosis; MRI; machine learning

1. Introduction

Currently, dual-energy X-ray absorptiometry (DXA) and quantitative-CT (QCT) are the standard methods for assessing bone mineral density (BMD). DXA is a widely available and relatively low-cost method that involves exposing the patient to low levels of radiation. However, DXA has limitations in its ability to assess trabecular bone density, and it does not provide information on bone quality. QCT provides comparable results to those of DXA but involves a higher radiation dose and is more expensive. Both methods are also limited by the fact that they only assess the bone mineral content and do not provide any information on the underlying bone structure [1].

Texture analysis can overcome some of these limitations and provide additional information about bone quality.

Textural analysis of MRI scans has been used in various fields, including radiology and oncology, to identify disease states and provide quantitative measures of disease progression [2]. In the case of bone health, texture analysis can be used to extract quantitative measures that reflect trabecular bone morphology, such as bone volume fraction, trabecular

thickness, and trabecular separation. Texture analysis can also reveal changes in bone structure that may not be apparent on DXA or QCT [3].

Recent studies have shown that texture analysis has potential as an alternative method for assessing BMD. For example, a study comparing texture analysis performed on lumbar spine MRI scans and DXA measurements found that trabecular bone texture features were significantly associated with DXA-derived BMD values [4].

Despite these promising results, texture analysis is not yet widely used in clinical practice for assessing BMD. More research is needed to validate its use as a diagnostic tool and to optimize the algorithms used to analyze the images.

Texture analysis is a method that involves quantitatively characterizing the patterns of intensity, contrast, and homogeneity in an image. These patterns can be used to infer underlying tissue characteristics, such as bone microarchitecture, which may not be readily visible to the naked eye.

Texture analysis methods can be broadly categorized into two types: first-order and higher-order features. First-order features are statistical descriptors derived from the distribution of pixel intensity values within an image, such as the mean, standard deviation, and entropy. These features provide an overall characterization of the image without directly capturing the spatial relationships between pixels. Higher-order features, on the other hand, are calculated from spatial relationships between pixel intensities and describe more complex patterns in an image. Examples of higher-order features include gray level co-occurrence matrix (GLCM)-based features, gray level run length matrix (GLRLM)-based features, and gray level size zone matrix (GLSZM)-based features [5]. These features capture information about the spatial arrangement of pixels and can provide more detailed information on the microstructure of bones. Higher-order texture features have shown promising results in characterizing changes in bone microarchitecture due to different bone disease states, such as osteoporosis, and may provide valuable information for early detection and diagnosis of such diseases.

Moreover, a study demonstrated that texture analysis can provide a predictive value on pathological fractures independently of BMD [6].

The aim of our study is to report our preliminary experience in the assessment of BMD via MRI-based textural analyses in a cohort of patients who have undergone DXA and lumbosacral MRIs, to assess the possibility of a standard examination to be able to opportunistically raise concern about osteoporosis.

2. Materials and Methods

2.1. Study Design

This is retrospective observational research. This study was conducted following the criteria set by the Declaration of Helsinki and further amendments.

We retrospectively reviewed all the lumbosacral MRIs from a 3rd level orthopedic hospital archive (from 2019 to 2021); then, we included those patients who were submitted for a lumbar DXA in our institution within 2 years from MRIs.

2.2. Study Population

Patients who underwent bot lumbar tract DXA and spine MRI in the last 2 years were selected from the institution's database, comprising a total of 881 MRI and 1793 DXA.

Exclusion criteria were the presence of metal artifacts, vertebral fracture incurring between DXA and MRI, and MRI acquired with a 3T scanner. Occurrence of menopause or beginning of treatments may influence BMD in the range of time between DXA and MRI.

Information regarding ge, sex, and time passed between the two examinations was collected.

2.3. DXA

The evaluation of the lumbar spine (L1–L4) was performed using the Hologic Explorer (Hologic, Bedford, MA, USA) with Apex system software (v4.6.0.7). Bone mineral density, Z-score, T-Score, and area of the vertebra were collected.

2.4. MRI

The MRI examination was performed with a 1.5 T scanner (Signa® 1.5 T, General Electric, Boston, MA, USA) that was equipped with a phased array spinal coil. T2w with and without fat saturation (FS), and T1w sequences were analyzed.

2.5. Texture Analysis

Texture analysis was performed using LifeX software (7.20). Volumes of interest were manually defined on the vertebral bodies of the L1–L4 tract of the lumbar spine by 1 radiologists (G.V.) with 5 years of experience in the field of musculoskeletal imaging. Intensity discretization was set on 256 grey levels, and intensity rescaling was set to the upper and lower bounds of the VOIs. All the available features were computed. Figure 1 depicts the regions of interest (ROIs) drawing method and the extraction of the local maps of 2nd order features.
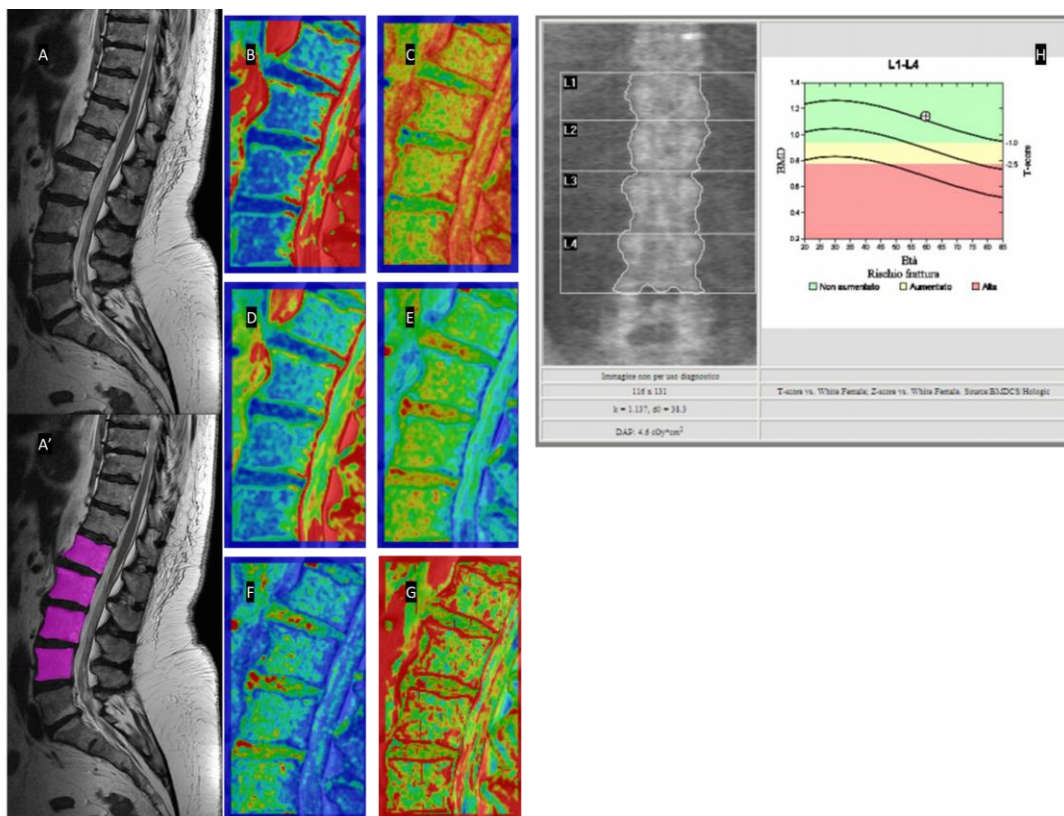
Figure 1. T2-w Lumbar spine MRI (**A**) with the ROIs (pink) placed on the tracts L1–L4 (**A'**). Rainbow-scale local maps representing contrast (**B**), entropy (**C**), dissimilarity (**D**), homogeneity (**E**), energy (**F**), and correlation (**G**). The DXA results for this patient are shown in panel (**H**).

2.6. Statistical Analysis

Statistical analysis was performed using IBM® SPSS® v25. Variable selection was performed using stepwise-forward method. A linear regression was performed between texture features and BMD. The Kruskal–Wallis test was used to compare distributions among healthy, osteopenic, and osteoporotic patients. The ROC curve was used to assess

accuracy of features in identifying healthy, osteopenic, and osteoporotic patients. A single layer perceptron (SLP) was built with 12 nodes with a training test ratio of 7:3.

3. Results

A total of 42 patients were selected, with 160 vertebral bodies suitable for the analysis. The selection process is shown in Figure 2.
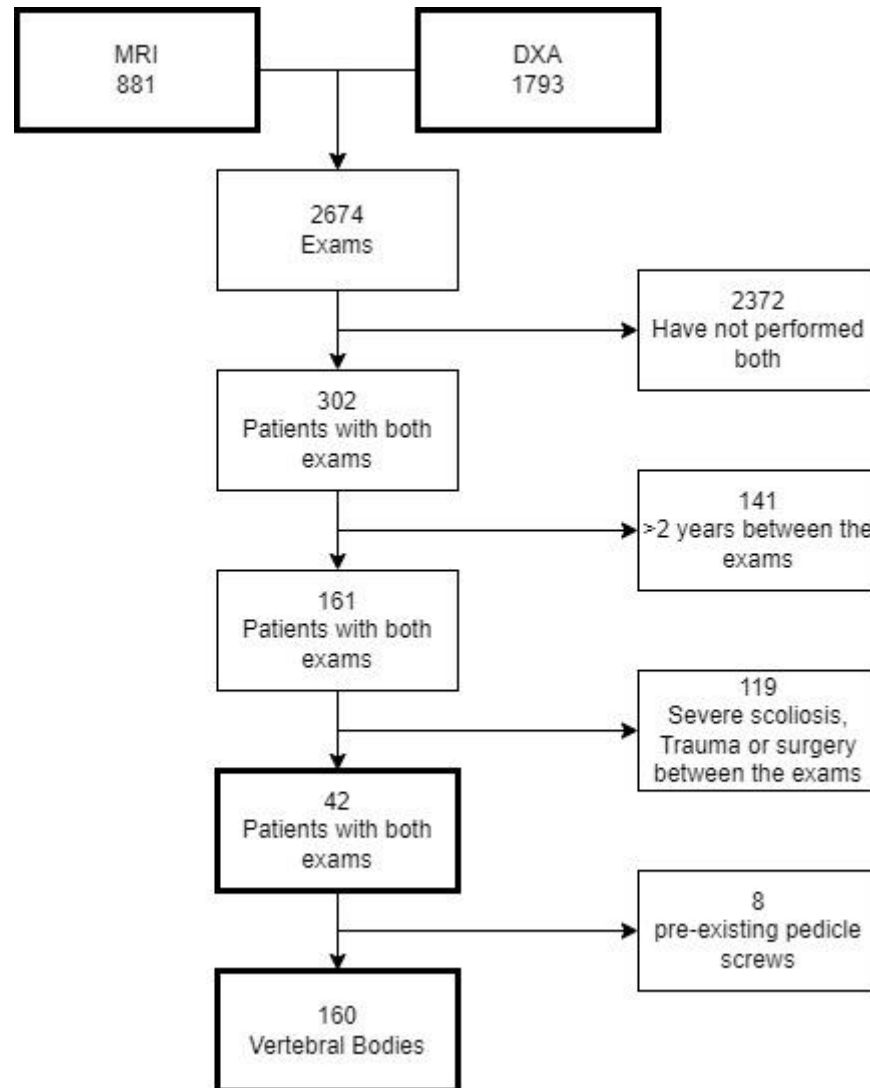
Figure 2. The PRISMA diagram illustrating patients' selection.

The selected patients were all females, with an average age of 70 (±10.8) years. Descriptive statistics of the results of the DXA of the population are shown in Table 1.

Table 1. Descriptive statistics of the study population.

	DXA DESCRIPTIVE STATISTICS			
	Minimum	**Maximum**	**Mean**	**Dev. Std.**
AREA	0.485	18.710	14.12411	2.331933
BMC	6.680	20.850	12.07048	3.296413
BMD	0.529	1.636	0.85173	0.219239
T-SCORE	−5.000	5.200	−1.64048	2.043687
PR	49.000	154.000	81.85714	20.961320
Z-SCORE	−3.800	8.100	0.22840	2.273391

3.1. Correlations between Radiomics MRI Features and BMD

In Table 2, correlations between radiomics MRI features and BMD are shown.

Table 2. Correlations between radiomics MRI features and BMD. The correlation index is followed by the significance (*p*) in parentheses. N.A. = Non Available, redundant; N.S. = Non significative.

Feature	T1	T2	T2 Fat-Sat
First Order			
Volume	0.226 (0.005)	N.A.	N.A.
Surface	0.228 (0.004)	N.A.	N.A.
Compacity	0.179 (0.026)	N.A.	N.A.
Conv. Min.	−0.173 (0.032)	N.S.	N.S.
Conv. Max	N.S.	−0.166 (0.039)	N.S.
Conv. Kurtosis	−0.261 (0.001)	−0.265 (0.001)	N.S.
Conv. Excess Kurt.	−0.340 (<0.001)	−0.265 (0.001)	N.S.
Disc. Standard Dev.	N.S.	0.224 (0.005)	0.344 (<0.001)
Disc. Q2	N.S.	0.183 (0.022)	0.169 (0.014)
Disc. Q3	N.S.	0.224 (0.005)	0.253 (0.001)
Histogram Energy	−0.205 (0.010)	−0.260 (0.001)	−0.247 (0.002)
Histogram Entropy	N.S.	0.199 (0.013)	0.265 (0.001)
GLCM			
Homogeneity	−0.205 (0.011)	−0.289 (<0.001)	−0.212 (0.008)
Contrast	N.S.	0.169 (0.036)	0.187 (0.020)
Entropy	0.250 (0.002)	0.280 (<0.001)	0.258 (0.001)
Dissimilarity	N.S.	0.231 (0.004)	0.227 (0.005)
GLRLM			
SRE	0.167 (0.038)	0.239 (0.003)	0.173 (0.031)
LRE	−0.169 (0.035)	−0.241 (0.003)	−0.170 (0.034)
HGRE	N.S	0.176 (0.028)	0.247 (0.001)
SRHGE	N.S	0.177 (0.028)	0.275 (0.001)
LRHGE	N.S	0.174 (0.031)	0.272 (0.001)
GLNU	N.S	N.S	−0.160 (0.047)
RP	0.168 (0.037)	0.240 (0.003)	0.172 (0.032)
GLZLM			
SZE	−0.176 (0.028)	0.216 (0.007)	0.159 (0.048)
HGZE	N.S	0.169 (0.036)	0.271 (0.001)
SZHGE	N.S	0.170 (0.034)	0.270 (0.001)
ZLNU	N.S	N.S	0.171 (0.033)
ZP	0.160 (0.046)	0.233 (0.004)	0.173 (0.032)
NGLDM			
Contrast	0.237 (0.003)	0.282 (<0.001)	0.228 (0.004)
PET/CT			
Agatston	N.S	N.S	−0.358 (0.013)
Peak Sphere 0.5 mL	N.S	N.S	0.266 (0.001)
Peak Sphere 1.0 mL	N.S	N.S	0.298 (<0.001)

3.2. Linear Regression Modeling on BMD

Features extracted from the T2 and the T2FS sequences showed significative coefficients in the linear regression for BMD; the resulting predicted values showed a correlation with BMD with correlation index of 0.640 ($p < 0.001$), F = 11.442, R^2 = 0.485. Coefficients are detailed in Table 3. The adjusted predicted values are shown in Figure 3, in a scatterplot with BMD.

Table 3. Linear regression for BMD.

|						
LINEAR REGRESSION FOR BMD						
FEATURE	**B**	**Std. Err.**	**t**	**Sign.**	**95% C.I.**	**Importance**
CONSTANT	29.560	11.620	2.544	0.012	6.675–52.445	
T2 DISC. HISTO. ENTR.	−6.516	0.898	−7.260	<0.001	−8.284−−4.749	0.169
T2 NGLDM CONTRAST	0.986	0.137	7.192	<0.001	0.716–1.256	0.165
T2 FS GLNU	−0.002	0.000	−5.813	<0.001	−0.001–0.108	0.108
T1 HISTO. ENERGY	−144.307	25.540	−5.650	<0.001	−194.607−−94.007	0.102
T1 MIN.	−0.001	0.001	−4.443	<0.001	−0.002−−0.001	0.063
T2 ZLNU	<0.001	<0.001	4.133	<0.001	0.000–0.000	0.055
T2 LZLGE	>−0.001	<0.001	−3.023	0.003	−0.000−−0.000	0.029
T2 FS DISSI.	−0.024	0.008	−2.834	0.003	−0.040−−0.008	0.028
T1 LZHGE	>−0.001	<0.001	−2.834	0.005	−0.000−−0.000	0.026
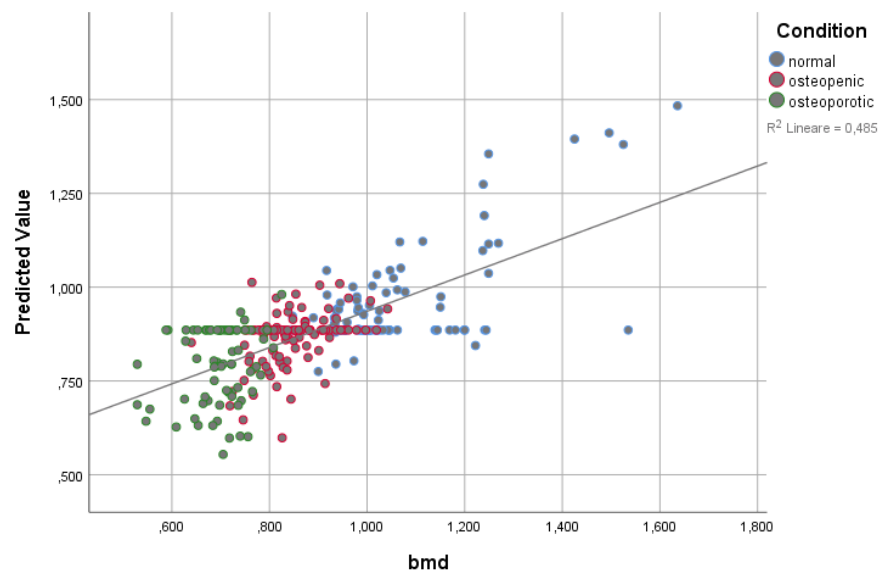
Figure 3. Cluster Scatterplot of the adjusted predicted values obtained by the linear model with the BMD.

Healthy, osteopenic, and osteoporotic patients showed significatively different predicted values with the Kruskal–Wallis test ($p < 0.001$) (Figure 4).
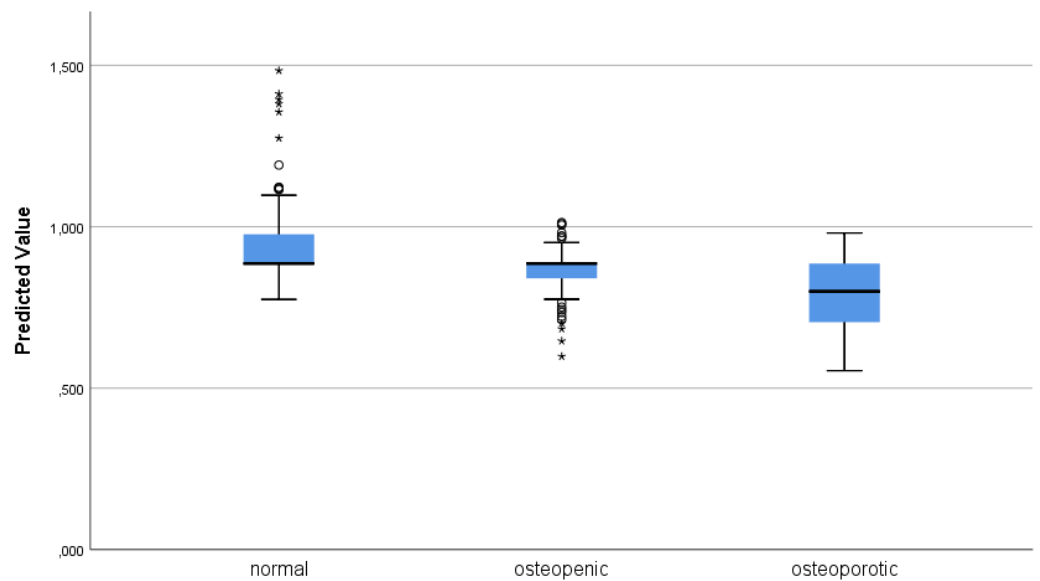
Figure 4. Box plot illustrating the adjusted predicted values of the linear regression model grouped by clinical population.

3.3. Single Layer Perceptron

The ML model improved the accuracy for the prediction of the BMD ($R^2 = 0.580$, $p < 0.001$) (Figure 5).
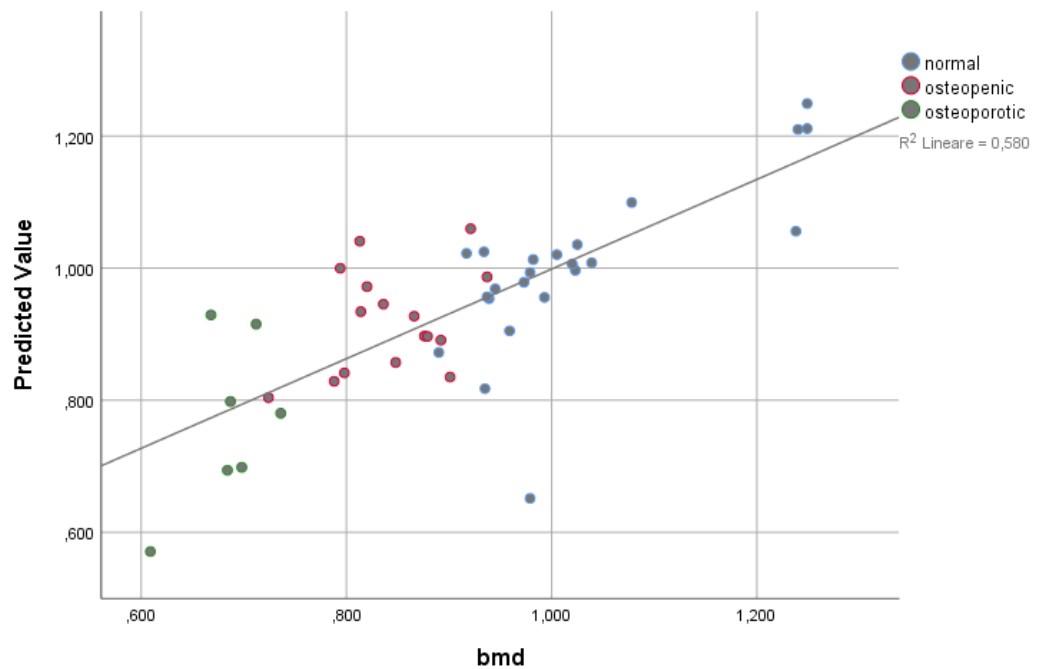
Figure 5. Cluster scatterplot of the adjusted predicted values obtained using the single-layer perceptron with the BMD.

It demonstrated significative accuracy when used with a nominal dependent variable, i.e., the clinical condition

The accuracy for training and test is reported in Table 4 and illustrated with a box-plot for the pseudoprobability of the predicted groups (Figure 6).

Table 4. The accuracy of the single-layer perceptron to predict the clinical condition, in the training and test cohorts.

		SLP			
		Predicted			
Sample		**Normal**	**Osteopenic**	**Osteoporotic**	**Correct**
Training	normal	21	0	0	100.0%
	osteopenic	1	10	0	90.9%
	osteoporotic	1	0	5	83.3%
	global perc.	60.5%	26.3%	13.2%	94.7%
Test	normal	2	0	0	100.0%
	osteopenic	0	5	0	100.0%
	osteoporotic	0	0	1	100.0%
	global perc.	25.0%	62.5%	12.5%	100.0%
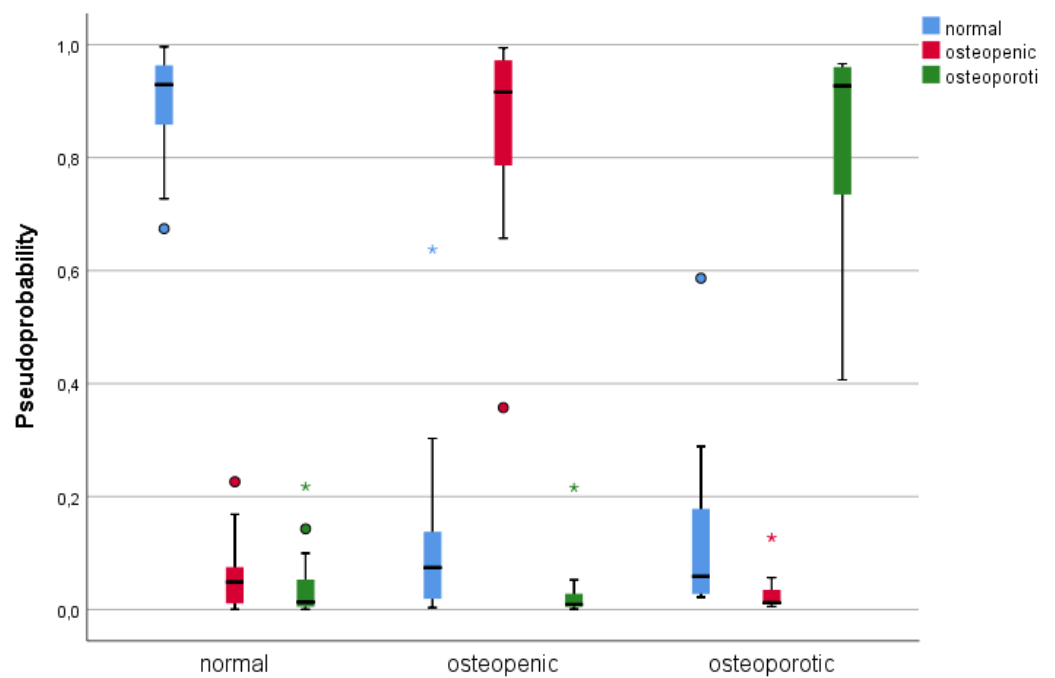
Figure 6. Box plot for the pseudoprobability of the predicted groups. Dots: values beyond 2 SD; *: outliers.

The cost function graph helps visualize how the sample is sufficient for the task, and the risk of overfitting is minimal (Figure 7).

The following table (Table 5) reports the normalized importance for each feature in the building of the model.
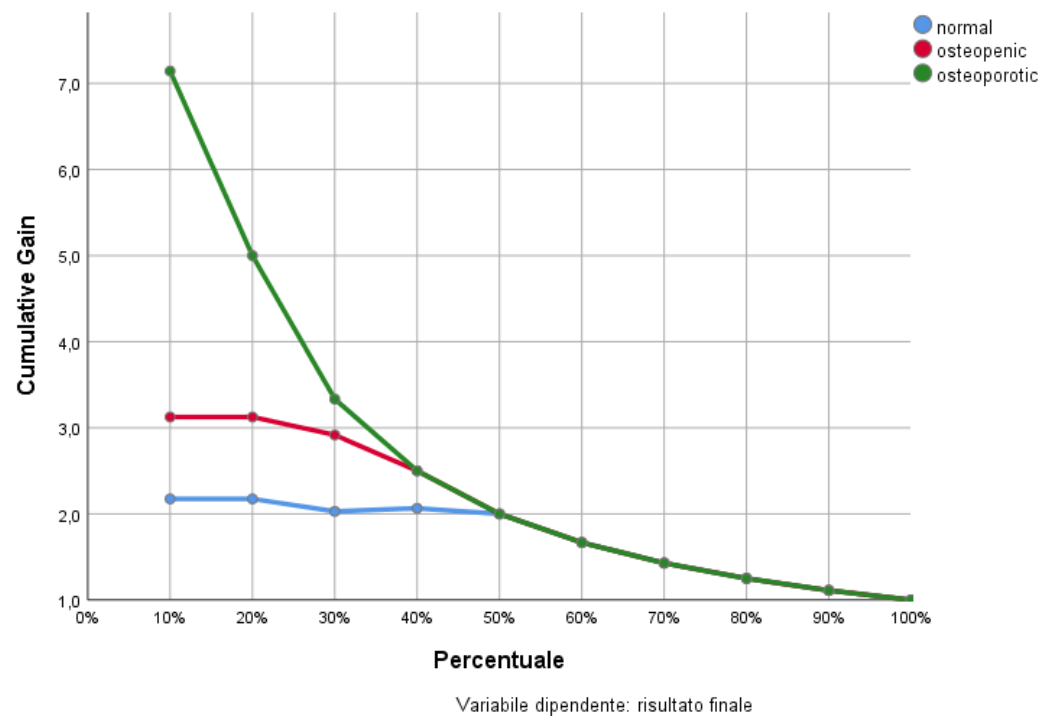
Figure 7. Gain function in subsequent training epochs.

Table 5. Normalized importance for each feature in the single-layer perceptron. Conditional formatting helps highlight the most important feature on each sequence. The background color of the cells is in a scale from green to red, to highlight the most (green) and least (red) important features.

Feature	T1	T2	T2FS	Shape	%
CONVENTIONAL_min	38.3%	36.8%	68.2%	SHAPE_Volume (mL)	31.2%
CONVENTIONAL_mean	32.9%	40.4%	29.3%	SHAPE_Volume (vx)	43.7%
CONVENTIONAL_std	46.8%	27.7%	28.6%	SHAPE_Sphericity	31.5%
CONVENTIONAL_max	28.0%	23.4%	43.7%	SHAPE_Surface (mm^2)	52.5%
CONVENTIONAL_Q1	27.9%	24.9%	40.0%	SHAPE_Compacity	23.1%
CONVENTIONAL_Q2	35.3%	30.9%	42.8%		
CONVENTIONAL_Q3	35.9%	35.2%	31.0%		
CONVENTIONAL_Skewness	43.3%	65.7%	69.5%		
CONVENTIONAL_Kurtosis	38.6%	58.8%	27.2%		
CONVENTIONAL_ExcessKurtosis	56.0%	52.9%	41.2%		
CONVENTIONAL_peakSphere0.5mL:discretized volume sought	34.1%	26.5%	27.1%		
CONVENTIONAL_peakSphere0.5mL(value only for PET or NM)	23.8%	35.7%	54.4%		
CONVENTIONAL_peakSphere1mL:discretized volume sought	28.9%	16.2%	46.8%		

Table 5. *Cont.*

Feature	T1	T2	T2FS	Shape	%
CONVENTIONAL_peakSphere1mL(value only for PET or NM)	45.5%	18.3%	32.4%		
CONVENTIONAL_calciumAgatstonScore[onlyForCT]	58.8%	30.8%	44.4%		
CONVENTIONAL_TLG (mL)[onlyForPETorNM]	35.2%	33.9%	19.4%		
DISCRETIZED_mean	47.9%	46.4%	67.2%		
DISCRETIZED_std	47.3%	59.4%	52.7%		
DISCRETIZED_Q1	48.2%	49.0%	53.5%		
DISCRETIZED_Q2	40.7%	39.0%	54.9%		
DISCRETIZED_Q3	25.2%	40.8%	59.8%		
DISCRETIZED_Skewness	31.5%	53.2%	55.5%		
DISCRETIZED_Kurtosis	43.4%	75.6%	64.0%		
DISCRETIZED_ExcessKurtosis	51.7%	43.4%	43.9%		
DISCRETIZED_peakSphere0.5mL:discretized volume sought	23.8%	40.5%	19.5%		
DISCRETIZED_peakSphere0.5mL (value only for PET or NM)	63.8%	43.0%	50.8%		
DISCRETIZED_peakSphere1mL:discretized volume sought	19.4%	30.1%	21.4%		
DISCRETIZED_peakSphere1mL (value only for PET or NM)	46.6%	36.4%	43.2%		
DISCRETIZED_TLG (mL) [onlyForPETorNM]	67.0%	60.8%	46.2%		
DISCRETIZED_HISTO_Entropy_log10	64.0%	50.4%	40.4%		
DISCRETIZED_HISTO_Entropy_log2	39.1%	40.3%	46.6%		
DISCRETIZED_HISTO_Energy [=Uniformity]	41.6%	51.9%	32.9%		
GLCM_Homogeneity [=InverseDifference]	46.6%	26.4%	26.4%		
GLCM_Energy [=AngularSecondMoment]	30.7%	18.9%	18.9%		
GLCM_Contrast [=Variance]	53.6%	39.9%	39.9%		
GLCM_Correlation	39.5%	49.1%	49.1%		
GLCM_Entropy_log10	39.0%	34.4%	34.4%		
GLCM_Entropy_log2 [=JointEntropy]	38.2%	38.7%	38.7%		
GLCM_Dissimilarity	47.5%	71.0%	71.0%		
GLRLM_SRE	32.7%	48.4%	48.4%		
GLRLM_LRE	44.8%	40.3%	40.3%		
GLRLM_LGRE	27.9%	36.1%	36.1%		
GLRLM_HGRE	34.4%	29.9%	29.9%		
GLRLM_SRLGE	27.8%	33.6%	33.6%		
GLRLM_SRHGE	44.2%	55.5%	55.5%		
GLRLM_LRLGE	67.9%	33.2%	33.2%		
GLRLM_LRHGE	33.7%	33.6%	33.6%		
GLRLM_GLNU	47.4%	36.5%	36.5%		
GLRLM_RLNU	50.3%	41.8%	41.8%		
GLRLM_RP	42.8%	34.1%	34.1%		
NGLDM_Coarseness	61.0%	45.8%	45.8%		
NGLDM_Contrast	63.6%	40.4%	40.4%		
NGLDM_Busyness	100.0%	32.9%	32.9%		
GLZLM_SZE	30.9%	50.5%	50.5%		
GLZLM_LZE	36.8%	51.8%	51.8%		
GLZLM_LGZE	17.3%	45.5%	45.5%		

Table 5. *Cont.*

Feature	T1	T2	T2FS	Shape	%
GLZLM_HGZE	37.3%	50.9%	50.9%		
GLZLM_SZLGE	27.6%	35.6%	35.6%		
GLZLM_SZHGE	48.9%	32.3%	32.3%		
GLZLM_LZLGE	27.4%	28.8%	28.8%		
GLZLM_LZHGE	20.3%	59.1%	59.1%		
GLZLM_GLNU	36.3%	31.8%	31.8%		
GLZLM_ZLNU	47.6%	54.1%	54.1%		
GLZLM_ZP	54.9%	39.5%	39.5%		

4. Discussion

Osteoporosis is a common skeletal disorder that is associated with increased morbidity and mortality worldwide. It is characterized by reduced bone density and increased risk of fracture, and its diagnosis and management require accurate assessment of bone mineral density (BMD). Dual-energy X-ray absorptiometry (DXA) is currently the gold standard for BMD assessment and osteoporosis diagnosis. DXA is a non-invasive imaging technique that uses low-dose X-rays to measure BMD at specific sites, particularly the distal forearm, the hip, and the lumbar spine for the diagnosis of osteoporosis [7].

Spinal disorders have a significant impact on radiology work and, as a result, on the entire healthcare system. MRI of the lumbar spine is currently ranked second (USD 686 million per year), after mammography (USD 718 million per year), in terms of total charges for imaging examinations in the United States [8]. Due to this, the application of a textural analyses for BMD assessment in lumbosacral MRI would have a huge impact on clinical practice, possibly avoiding further unnecessary examinations.

Texture analysis (TA) is a computerized method for quantifying the spatial distribution and heterogeneity of image intensities in MRI images. In the context of bone mineral density (BMD) assessment, TA can be used to analyze the texture of the trabecular bone and bone marrow in MRI images of the lumbar spine.

One of the main challenges in using MRI for TA is the presence of noise in the images. MRI is inherently noisy due to several factors, including the low signal-to-noise ratio (SNR) of the images and the presence of artifacts such as motion and susceptibility artifacts. This noise can affect the accuracy of TA parameters, particularly those that rely on the spatial distribution of image intensities. In contrast, CT images typically have higher SNR and less noise, which can make TA analysis more robust and accurate [9].

Another challenge in using MRI for TA is the complex nature of the MRI signal. Unlike CT, which provides a direct measure of X-ray attenuation, MRI measures the relaxation times of protons in tissue. This signal can be influenced by numerous factors, including the tissue composition, magnetic field inhomogeneities, and imaging parameters. These factors can affect the accuracy and reproducibility of TA parameters derived from MRI [10].

Furthermore, the acquisition and processing of MRI images can be more time-consuming and technically challenging compared to CT. MRI typically requires longer acquisition times, and the images must be processed to correct for motion artifacts and other sources of image distortion. This processing can introduce additional variability and noise into the images, which can affect the accuracy of TA parameters [10].

To increase the reliability of texture analysis (TA) features derived from magnetic resonance imaging (MRI) for bone mineral density (BMD) assessment, several approaches can be employed. The following include some of these:

1. Image quality control: It is important to ensure that the MRI images used for TA analysis are of high quality and free of artifacts such as motion or susceptibility artifacts. This can be achieved by implementing quality control measures such as visual inspection, automated motion correction algorithms, and coil sensitivity correction.

2. Reproducible image acquisition: Reproducibility of MRI acquisition is critical for reliable TA analysis. To achieve this, it is essential to use standardized protocols for MRI acquisition, including imaging parameters, patient positioning, and scanner calibration.
3. Automated segmentation: Accurate segmentation of bone and bone marrow regions in MRI images is essential for reliable TA analysis. Manual segmentation is subject to inter- and intra-observer variability, which can affect the reproducibility of TA features. Automated segmentation algorithms, such as thresholding or machine learning-based methods, can improve the accuracy and reproducibility of segmentation.
4. Standardized TA parameters: There are many different TA features that can be derived from MRI images, and the choice of features can affect the reliability and reproducibility of BMD assessment. To address this issue, it is important to use standardized TA parameters that have been validated in previous studies.
5. Calibration phantoms: Calibration phantoms can be used to ensure that the MRI images are consistent across different scanners and imaging protocols. These phantoms contain known concentrations of water and/or oil, and their signal intensity can be used to calibrate the MRI images.
6. Multi-site studies: Multi-site studies involving different MRI scanners and patient populations can help to validate the reliability and reproducibility of TA features. By comparing the results from different scanners and patient cohorts, the robustness and generalizability of TA features can be evaluated.

In summary, several approaches can be used to increase the reliability of TA features derived from MRI for BMD assessment. These include image quality control, reproducible image acquisition, automated segmentation, standardized TA parameters, calibration phantoms, and multi-site studies [11].

Dual-energy X-ray absorptiometry (DXA) is the gold standard for BMD assessment, and it measures the attenuation of X-rays passing through the bone. DXA provides a two-dimensional image of the bone and reports the BMD as grams of mineral per square centimeter (g/cm^2). DXA is widely used because it is reliable, non-invasive, and has a low radiation dose.

Several studies have investigated the correlation between TA on MRI and DXA for BMD assessment. Overall, the results suggest that TA can provide additional information about bone quality beyond what DXA measures. For example, TA can quantify the heterogeneity of the trabecular bone and bone marrow, which may be important for predicting fracture risk.

Some studies have reported a moderate to strong correlation between TA-derived parameters and DXA-derived BMD measurements. However, the strength of the correlation varies depending on the TA parameters and DXA sites analyzed. For instance, a study by Maciel et al. (2020) found a moderate correlation between TA parameters and DXA-derived BMD measurements at the lumbar spine [12].

This study reports comparable results; however, the correlation is stronger when analyzed with the appropriate model: machine learning can help greatly when dealing with many variables with unknown relationships. However, the appropriate model selection can impact the accuracy of the prediction [13].

In this study, the single-layer perceptron was used, for the relative simplicity of the architecture and the possibility to oversee the training and test phases, monitoring the gain/cost function, to help prevent overfitting [14].

According to Poullain et al. [4], GLNU and entropy hold significant value in predicting BMD from an opportunistic use of a conventional MRI scan. This study confirms this result when adopting the linear regression modelling; yet, in the multilayer perceptron approach, the NGLDM busyness appears to be more important. However, this feature describes a semantically similar property of the image, thus not deviating conceptually from the previously reported results.

Moreover, the direct relationship between entropy and BMD is demonstrated by Knoepflin et al. [3]. Even if the ultra-high field MRI employed in their study cannot pave

the way for an opportunistic use in clinical practice, the reported result helps to establish entropy as a core feature related to BMD. Lumbar MRI is a routine exam performed in patients with low back pain, and is widely available, representing no extra cost for the retrospective analysis (apart from the human processing time).

In all the procedures applied, it was evident that T2-weighted sequences yield more information than the others. The authors suggest basing upon these sequences further studies on the topic. The superiority of T2-w sequences on other topics has already been established by Crombé et al. [15].

Specific MRI sequences, such as T2* Mapping, could help better study the bone structure; however, they would require additional time to study. When evaluating the images retrospectively, T2-w sequences are widely available. Nonetheless, T2* Mapping could be considered when encountering a newly onset insufficiency fracture during the execution of the exam.

This study presents some limitations. Texture analysis can be heavily influenced by other conditions not strictly related to BMD: the presence of spinal hemangiomas or lymphoma could alter the derived features. Moreover, an heterogeneous population of males and female is needed to achieve more solid results. Finally, this study is retrospective, and a prospective follow-up of the presented cohort is necessary to test the potential of texture analysis to represent a risk factor for possible fractures.

In summary, while there is evidence of a correlation between TA on MRI and DXA for BMD assessment, the strength of the correlation may vary depending on the specific TA parameters and DXA sites analyzed. Nonetheless, TA may provide valuable information beyond what DXA measures and could be a useful adjunct for BMD assessment in certain patient populations.

Author Contributions: Conceptualization, G.V. (Giulio Vara) and F.U.; methodology, S.R., G.V. (Gianfranco Vornetti) and L.S.; software, G.V. (Giulio Vara) and P.S.; validation, M.M., G.V. (Giulio Vara) and F.U.; formal analysis, G.V. (Giulio Vara); investigation, G.V. (Giulio Vara); resources, M.M. and G.F.; data curation, G.V. (Giulio Vara); writing—original draft preparation, G.V. (Giulio Vara); writing—review and editing, P.S.; visualization, L.S. and S.R.; supervision, S.R. All authors have read and agreed to the published version of the manuscript.

Institutional Review Board Statement: Ethical review and approval were waived for this study due to the retrospective nature.

Informed Consent Statement: Informed consent was waived due to the retrospective nature of the study.

Data Availability Statement: Data are available upon request from the corresponding author.

Conflicts of Interest: The authors declare no conflict of interest.

References

1. Guerri, S.; Mercatelli, D.; Aparisi Gómez, M.P.; Napoli, A.; Battista, G.; Guglielmi, G.; Bazzocchi, A. Quantitative Imaging Techniques for the Assessment of Osteoporosis and Sarcopenia. *Quant. Imaging Med. Surg.* **2018**, *8*, 60–85. [CrossRef] [PubMed]
2. Shur, J.D.; Doran, S.J.; Kumar, S.; Ap Dafydd, D.; Downey, K.; O'Connor, J.P.B.; Papanikolaou, N.; Messiou, C.; Koh, D.-M.; Orton, M.R. Radiomics in Oncology: A Practical Guide. *Radiographics* **2021**, *41*, 1717–1732. [CrossRef] [PubMed]
3. Knoepflin, P.; Pithioux, M.; Bendahan, D.; Poullain, F.; Le Corroller, T.; Fabre, C.; Pauly, V.; Creze, M.; Soldati, E.; Champsaur, P.; et al. Texture Parameters Measured by UHF-MRI and CT Scan Provide Information on Bone Quality in Addition to BMD: A Biomechanical Ex Vivo Study. *Diagnostics* **2022**, *12*, 3143. [CrossRef] [PubMed]
4. Poullain, F.; Champsaur, P.; Pauly, V.; Knoepflin, P.; Le Corroller, T.; Creze, M.; Pithioux, M.; Bendahan, D.; Guenoun, D. Vertebral Trabecular Bone Texture Analysis in Opportunistic MRI and CT Scan Can Distinguish Patients with and without Osteoporotic Vertebral Fracture: A Preliminary Study. *Eur. J. Radiol.* **2023**, *158*, 110642. [CrossRef] [PubMed]
5. Tuceryan, M.; Jain, A.K. Texture Analysis. In *Handbook of Pattern Recognition and Computer Vision*; World Scientific: Singapore, 1993; pp. 235–276. ISBN 978-981-02-1136-3.

6. Benhamou, C.L.; Poupon, S.; Lespessailles, E.; Loiseau, S.; Jennane, R.; Siroux, V.; Ohley, W.; Pothuaud, L. Fractal Analysis of Radiographic Trabecular Bone Texture and Bone Mineral Density: Two Complementary Parameters Related to Osteoporotic Fractures. *J. Bone Miner Res.* **2001**, *16*, 697–704. [CrossRef] [PubMed]

7. Bazzocchi, A.; Ponti, F.; Albisinni, U.; Battista, G.; Guglielmi, G. DXA: Technical Aspects and Application. *Eur. J. Radiol.* **2016**, *85*, 1481–1492. [CrossRef] [PubMed]

8. Ballane, G.; Cauley, J.A.; Luckey, M.M.; El-Hajj Fuleihan, G. Worldwide Prevalence and Incidence of Osteoporotic Vertebral Fractures. *Osteoporos. Int.* **2017**, *28*, 1531–1542. [CrossRef]

9. Varghese, B.A.; Cen, S.Y.; Hwang, D.H.; Duddalwar, V.A. Texture Analysis of Imaging: What Radiologists Need to Know. *Am. J. Roentgenol.* **2019**, *212*, 520–528. [CrossRef]

10. Park, J.E.; Park, S.Y.; Kim, H.J.; Kim, H.S. Reproducibility and Generalizability in Radiomics Modeling: Possible Strategies in Radiologic and Statistical Perspectives. *Korean J. Radiol.* **2019**, *20*, 1124–1137. [CrossRef] [PubMed]

11. Orlhac, F.; Eertink, J.J.; Cottereau, A.-S.; Zijlstra, J.M.; Thieblemont, C.; Meignan, M.; Boellaard, R.; Buvat, I. A Guide to ComBat Harmonization of Imaging Biomarkers in Multicenter Studies. *J. Nucl. Med.* **2022**, *63*, 172–179. [CrossRef] [PubMed]

12. Maciel, J.G.; Araújo, I.M.D.; Trazzi, L.C.; Azevedo-Marques, P.M.D.; Salmon, C.E.G.; Paula, F.J.A.D.; Nogueira-Barbosa, M.H. Association of Bone Mineral Density with Bone Texture Attributes Extracted Using Routine Magnetic Resonance Imaging. *Clinics* **2020**, *75*, e1766. [CrossRef] [PubMed]

13. Spagnoli, L.; Morrone, M.F.; Giampieri, E.; Paolani, G.; Santoro, M.; Curti, N.; Coppola, F.; Ciccarese, F.; Vara, G.; Brandi, N.; et al. Outcome Prediction for SARS-CoV-2 Patients Using Machine Learning Modeling of Clinical, Radiological, and Radiomic Features Derived from Chest CT Images. *Appl. Sci.* **2022**, *12*, 4493. [CrossRef]

14. Moutarde, H.; Sznajder, P.; Wagner, J. Unbiased Determination of DVCS Compton Form Factors. *Eur. Phys. J. C* **2019**, *79*, 614. [CrossRef]

15. Crombé, A.; Périer, C.; Kind, M.; De Senneville, B.D.; Le Loarer, F.; Italiano, A.; Buy, X.; Saut, O. T2-based MRI Delta-radiomics improve response prediction in soft-tissue sarcomas treated by neoadjuvant chemotherapy. *J. Magn. Reson Imaging* **2019**, *50*, 497–510. [CrossRef] [PubMed]